Intermittent dynamics and logarithmic domain growth during the spinodal decomposition of a glass-forming liquid

Vincent Testard, Ludovic Berthier, Walter Kob

Intermittent dynamics and logarithmic domain growth during the spinodal decomposition of a glass-forming liquid

Vincent Testard, Ludovic Berthier, and Walter Kob
Laboratoire Charles Coulomb, UMR 5221 CNRS and Université Montpellier 2, 34095 Montpellier, France
(Dated: September 25, 2018)

We use large-scale molecular dynamics simulations of a simple glass-forming system to investigate how its liquid-gas phase separation kinetics depends on temperature. A shallow quench leads to a fully demixed liquid-gas system whereas a deep quench makes the dense phase undergo a glass transition and become an amorphous solid. This glass has a gel-like bicontinuous structure that evolves very slowly with time and becomes fully arrested in the limit where thermal fluctuations become negligible. We show that the phase separation kinetics changes qualitatively with temperature, the microscopic dynamics evolving from a surface tension-driven diffusive motion at high temperature to a strongly intermittent, heterogeneous and thermally activated dynamics at low temperature, with a logarithmically slow growth of the typical domain size. These results shed light on recent experimental observations of various porous materials produced by arrested spinodal decomposition, such as nonequilibrium colloidal gels and bicontinuous polymeric structures, and they elucidate the microscopic mechanisms underlying a specific class of viscoelastic phase separation.

I. INTRODUCTION

The behavior found in nonequilibrium kinetic phenomena such as self-assembly [1], pattern formation [2], and phase ordering kinetics [3] is typically much richer than the one encountered in equilibrium since a broader range of morphologies and a more complex relaxation dynamics can be observed in systems that are far from equilibrium. While this has been an active research area since many decades [2, 4], the field has seen a surge of interest in the last few years, since progress in the synthesis of colloidal particles with complex shapes and tunable pairwise interactions permits the self-assembly of materials of ever growing complexity, i.e. systems that exist only if one masters their intricate formation process [1].

One of the most important phenomenon occurring in nonequilibrium systems is spinodal decomposition [3, 5]. The case of shallow temperature quenches has been studied in great detail using theory as well as experiments. Various regimes for the time evolution of the average domain size have been predicted, and observed in controlled experiments and simulations of simple fluids using a multitude of computational approaches [6–10]. However, a much greater complexity can be expected if the dense phase is not a simple liquid [11] but is itself a "complex" fluid [12]. Of particular importance is the so-called "viscoelastic phase separation" [13, 14] which is characterized by a strong physical (mainly, rheological) asymmetry between the two coexisting phases. For instance, one can study the phase separation between two fluids of unequal viscosities, or the coexistence between a solid and a fluid phase. In the following we shall be concerned with a situation intermediate between these two, where one component will evolve from being a simple fluid to become a highly viscous liquid or an amorphous glass phase, thus giving rise to the phenomenon of a *glass-gas phase separation* [15–18].

The phase ordering process between a fluid and an amorphous solid can be expected to display a complex phenomenology, since even the equilibrium bulk behavior of (homogeneous) amorphous glasses is not well understood [19, 20]. When suddenly quenched from high temperature to below the glass temperature, a glass-forming material evolves slowly with time, undergoing a nonstationary aging dynamics characterized by intermittent, heterogeneous dynamics occurring far from equilibrium [20–24]. It is not clear how this aging glass state will evolve if it is given by the dense phase in the complex bicontinuous structure formed during spinodal decomposition. Since a glass behaves mechanically like a solid, one can expect that the bicontinuous structure formed after the quench into the coexistence region becomes rigid, and as a result will become kinetically arrested into a bicontinuous porous structure [16]. In that case, the glass-gas phase separation would thus be a conceptually very simple way of producing porous media. However, one can also expect that the aging of the glass phase enables intermittent, thermally activated microscopic rearrangements, which could potentially make the porous material very fragile. To advance our understanding regarding these questions we present here the results of our study concerning the interplay between phase separation kinetics and aging behavior resulting from deep quenches at low temperatures in a simple glass-forming model.

Although our main motivation is to obtain a fundamental understanding of the glass-gas phase separation kinetics, there are also several experimental considerations that motivate such a study. Firstly, a number of colloidal systems and protein solutions can be modelled as spherical particles with nearly hard-core repulsion and longer-ranged attraction, whose range and strength can be controlled. Thus, they will undergo a phase separation in some part of the phase diagram, which might possibly interfere with the colloidal glass formation occurring at higher densities. Therefore, the idea that, at least in some materials, gelation results from a kinetically arrested glass-gas spinodal decomposition has been explored in several experimental works [25–33]. This pro-

cess has also been the subject of a number of numerical studies, mostly aimed at reproducing realistic coarse-grained pair interactions characterizing colloidal systems that were specifically studied experimentally [27, 34–39]. More recent studies, in line with our own work [15], have considered more diverse systems, such as the phase separation kinetics of a coarse-grained model for buckyball C_{60} carbon molecules [40]. Moreover, bicontinuous disordered structures reminiscent of the ones obtained in spinodal decompositions may also be found in colorful bird feathers, and were recently interpreted as incompletely phase separated polymeric glasses [41, 42], thus demonstrating the broad relevance of the problem of the glass-gas phase separation. Finally, even more complex mixtures that are relevant to food processing [43] or solar cell technology [44–46] also exhibit kinetically arrested spinodal decompositions, that might result from the fact that one component becomes mechanically rigid.

There are several possible ways to study coarsening processes by means of theory [3]. One efficient approach is to study a coarse-grained model of a biphasic material using a Ginzburg-Landau free energy functional of the two-phase system complemented with phenomenological dynamical equations to incorporate relevant dynamical and mechanical properties of each phase [13, 47]. For simple fluids, this amounts to studying model H in the classification scheme proposed by Hohenberg and Halperin [4]. Possible extensions to viscoelastic materials have indeed been considered in the past [13], and numerically integrated to obtain insights into some specific viscoelastic phase separation processes. Still, it remains difficult to faithfully incorporate in this approach the complex (typically highly nonlinear and history dependent) physical properties of real glass-forming materials in their aging regime. Moreover, such coarse-grained equations cannot provide direct information on the microscopic dynamics responsible for the evolution of such bicontinuous materials.

To avoid this drawback we use here a microscopically realistic description of the homogeneous glass using an atomistic model combined with molecular dynamics techniques. We study its behavior during phase separation over a broad range of control parameters, mainly density and temperature. Indeed, numerous successful atomic-scale simulations of the simpler situation of a liquid-gas spinodal decomposition have been reported [6, 8, 48, 49]. In Ref. [50], a Lennard-Jones system was quenched to low temperature in the coexistence region, and the resulting crystal-gas phase separation was studied, but no kinetic arrest was reported (see Ref. [51] for a recent related experimental study). Simulations of realistic colloidal interactions have been reported in Refs. [34, 35, 37, 38], but the quenches have been performed to very low temperatures and hence particles aggregate nearly irreversibly and thermal fluctuations play little role, which corresponds effectively to zero-temperature quenches in our approach. Thus, a careful study of the crossover regime between ordinary spinodal decomposition and irreversible aggregation is so far not available.

In this work, we fill this gap and provide a detailed numerical study of the phase separation kinetics between a gas and a glass-forming material at various temperatures encompassing the glass transition of the bulk material. We describe how the phase separation kinetics changes qualitatively with temperature, the microscopic dynamics evolving from the well-known diffusive motion driven by surface tension for shallow quenches, to a qualitatively different coarsening regime in which dynamics becomes strongly intermittent, spatially heterogeneous and thermally activated at low temperature, leading to logarithmically slow growth of the typical domain size. A short account of our results has been published [15].

Our paper is organized as follows. In Sec. II we define the model, provide technical details about our numerical simulations, and discuss the phase diagram of the system and the relevant parameters to be explored in this work. In Sec. III we provide a qualitative description of the temperature influence on the spinodal decomposition kinetics. In Sec. IV we present several structural characterizations of the bicontinuous structures and in Sec. V we discuss the time evolution of these structures, characterizing in detail the influence of temperature on the growth law. In Sec. VI we provide insights into the microscopic mechanisms responsible for the coarsening structures at high and low temperatures. In Sec. VII we discuss the nature of the coexistence line below the glass transition temperature, that was the subject of a recent controversy in the literature. In Sec. VIII, we close the paper with some perspectives for future work.

II. MODEL AND PHASE DIAGRAM

In this section, we describe details of the Lennard-Jones model used in this study and provide some technical informations about the numerical simulations. We then describe the relevant features of the phase diagram of the model. Finally we introduce a coarse-grained density field that will be useful to the analysis of the simulations.

A. Model and technical details

To study the interplay between liquid-gas phase separation and the liquid-glass transition we consider a simple Lennard-Jones model for a liquid that was first devised to study the dynamics of glass-forming materials in the bulk [52]. The model is a 80:20 binary mixture of Lennard-Jones particles with asymmetric interaction parameters chosen such that the minority component frustrates, and therefore efficiently prevents, the crystallization of the majority component. The details of the interaction parameters are as in the original publication [52]. In the following we use Lennard-Jones units corresponding to the majority component, express-

ing length in units of the particle diameter, σ, and time in units of $\tau = \sqrt{m\sigma^2/\epsilon}$, where m is the particle mass and ϵ the energy scale of the Lennard-Jones interaction between particles of the majority component.

We integrate Newton's equation of motion using LAMMPS [53] for N particles enclosed in a volume V, working with periodic boundary conditions. We work at constant number density, $\rho = N/V$, and adjust the temperature T using periodic velocity rescaling as a simple thermostatting procedure. The equations of motion are integrated using a standard velocity Verlet scheme, using a discretization time step of 0.01 in reduced Lennard-Jones units.

To study the kinetics of phase separation, we first prepare homogeneous samples at the desired density ρ, working at high temperature, $T = 3.0$, well above the critical point $T_c \approx 1.2$, until thermal equilibrium is reached. We then instantaneously quench the temperature T to the desired final value, where the phase separation dynamics starts. In the following we will denote as the "age" of the system the time elapsed since the quench to the final temperature. To improve the statistics of our quantitative measurements and the robustness of our findings, we have repeated simulations at each state point using 5 to 10 samples, using independently prepared samples at high temperatures.

Specific attention has been paid to system size. While numerical studies of the glass transition in the homogeneous liquid typically require simulating about $N = 10^3$ particles, we have found that up to $N = 10^6$ particles are needed to obtain results devoid of finite size effects during the phase separation. We have obtained most of our quantitative results using $N = 3 \cdot 10^5$ particles. Where appropriate, we will discuss the N-dependence of our numerical results.

B. Coarse-graining the density

Since the bicontinuous structures produced during a spinodal decomposition are characterized by a typical length scale that is often much larger than the typical particle size, the local structure of the fluid is largely irrelevant. Therefore, it will prove useful to first coarse-grain the density field before quantifying the spatial fluctuations of the obtained field [54, 55]. This coarse-grained density will also be used to facilitate the visualizations of the particle configurations.

We start from the microscopic density field, which is defined as

$$\rho_{\rm micro}(\mathbf{r}) = \sum_{i=1}^{N} \delta(\mathbf{r} - \mathbf{r}_i), \qquad (1)$$

where $\mathbf{r}_i$ is the position of particle i. Our first step is to discretize space by dividing it into boxes of linear size $\xi_{\rm b}$, so that continuous space is now replaced by a discrete lattice containing $V/\xi_{\rm b}^3$ sites. We consider a discrete density, $\rho(\mathbf{r})$, defined for discrete positions $\mathbf{r}$ located at the center of the boxes described above, as

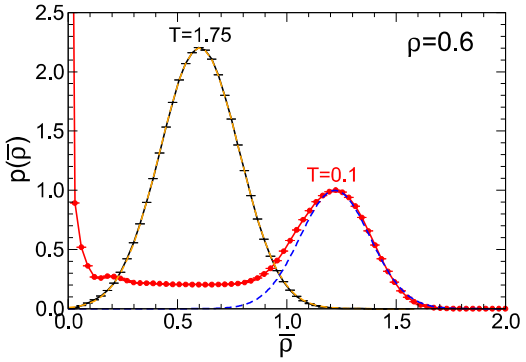

FIG. 1: Probability distribution function of the coarse-grained density field for $\rho = 0.6$ for both a homogeneous fluid configuration at $T = 1.75$ and for a phase separating system at $T = 0.1$. The dashed lines are a fit with a Gaussian.

$$\rho(\mathbf{r}) = \frac{3}{4\pi\xi_{\rm s}^3} \sum_{i=1}^{N} \theta(\xi_{\rm s} - |\mathbf{r} - \mathbf{r}_i|), \qquad (2)$$

where $\theta(x)$ is the Heaviside function and a second coarse-graining length, $\xi_{\rm s}$, is introduced. Thus, the density at position $\mathbf{r}$ takes into account all particles located in a sphere of radius $\xi_{\rm s}$ centered at $\mathbf{r}$.

Finally, we obtain the desired coarse-grained density $\bar{\rho}(\mathbf{r})$ by using the following weighted average of $\rho(\mathbf{r})$ over the boxes surrounding $\mathbf{r}$:

$$\begin{aligned}\bar{\rho}(\mathbf{r}) \;=\; & \frac{1}{8}\big[2\rho(\mathbf{r}) + \rho(\mathbf{r} + \xi_b\mathbf{e}_x) + \rho(\mathbf{r} + \xi_b\mathbf{e}_y) + \rho(\mathbf{r} + \xi_b\mathbf{e}_z) \\ & + \rho(\mathbf{r} - \xi_b\mathbf{e}_x) + \rho(\mathbf{r} - \xi_b\mathbf{e}_y) + \rho(\mathbf{r} - \xi_b\mathbf{e}_z)\big]. \qquad (3)\end{aligned}$$

Here $\mathbf{e}_\alpha$ is a unit vector in direction α.

The procedure described by Eqs. (2, 3) is easy to implement. It returns for each lattice site a coarse-grained density field which is a much smoother function than the microscopic density field $\rho_{\rm micro}(\mathbf{r})$ in Eq. (1). The two coarse-graining length scales $\xi_{\rm b}$ and $\xi_{\rm s}$ can be adjusted by seeking a compromise between having a smooth field without losing too much spatial resolution. After having tried several combinations [56], we have settled to the values $\xi_{\rm b} = \sigma/2$ and $\xi_{\rm s} = \sigma$, so that the lattice spacing is equal to the particle radius, while the density field is coarse-grained by taking into account the immediate neighbourood of each particle.

Having defined the coarse-grained density field $\bar{\rho}(\mathbf{r})$, we can now easily transform a set of particle coordinates from a single particle configuration into the probability distribution of the coarse-grained density, $p(\bar{\rho})$. In Fig. 1, we show this distribution for two configurations obtained

at density $\rho = 0.6$. The first example is measured for $T = 1.75$, where the system is in the homogeneous fluid phase. As shown by the dashed line, the distribution is well described by a Gaussian functional form with a maximum located at $\bar{\rho} = 0.6$, as expected. More interesting is the second case at $T = 0.1$ where the system is in the phase coexistence region. For this low temperature, complete phase separation is not reached. The distribution $p(\bar{\rho})$ directly reflects this phase coexistence, since it is characterized by two peaks. One peak is located at very low density, representative of the gas phase (whose very small density is not resolved in the scale chosen in Fig. 1). A second peak corresponds to the dense phase and has a maximum near $\rho \approx 1.2$ in this specific example. In between these peaks, the distribution is nearly flat. We checked that this intermediate density band corresponds to sites located near the interfaces between the two phases where the density can take any value comprised between the ones of the gas and fluid phases.

These observations can be used for two purposes: First, by adjusting the peak at high density to a Gaussian distribution, we can directly measure the average density of the dense phase and follow its evolution during a quench to the coexistence region. This will be used for instance in Sec. VII to determine the coexistence line at low temperature where complete phase separation is not reached at long times, see also the binodal curve in the phase diagram of Fig. 2.

A second application is the possibility to clearly distinguish, using $\bar{\rho}$ and $p(\bar{\rho})$, between cells that belong to either of the two phases, and those belonging to the interfaces. To this end, we need to determine a threshold density delimiting the dense phase from the gas phase. By careful visual inspections of several configurations at various state points, we have chosen $\bar{\rho} = 0.42$ as giving the most faithful representation of the particle configurations. Thus, we define from now on cells with $\bar{\rho} > 0.42$ as belonging to the fluid phase, and cells with $\bar{\rho} < 0.42$ as those forming the gas phase. Interfaces are represented by cells that are in the dense phase and that have at least one neighboring cell that is *not* in the dense phase. We have used for instance these definitions to produce the images shown in Figs. 4 and 5, where only cells belonging to the interfaces were shown, using different colors for gas and fluid phases.

C. Phase diagram

Using a combination of direct visual inspection of equilibrium configurations coupled to more quantitative methods to analyze the morphology of biphasic atomistic configurations (as described above), we have determined the phase diagram shown in Fig. 2, which we complement with some relevant literature data. In this phase diagram, the control parameters are the temperature, T, and the number density, ρ.

When density is high enough, roughly $\rho \geq 1.2$, the system is always homogeneous. Similarly, the system is a homogeneous fluid at high temperature, $T \geq T_c \approx 1.2$, which corresponds to the critical temperature. At large density and temperature, the system is a simple liquid, but its dynamics slows down dramatically as temperature decreases, without showing sign of crystallization. Therefore, the system undergoes a glass transition from a viscous liquid to an amorphous glass as temperature is decreased at constant density. This process has been extensively studied before [52]. To set the typical temperature scale for the glass formation, we include in Fig. 2 the density dependence of the temperature obtained by analyzing the dynamics in the framework of the mode-coupling theory of the glass transition [57]. This temperature was determined by a power-law fit to the growth of the equilibrium relaxation time. It is known to represent a useful temperature scale below which it becomes difficult to reach thermal equilibrium in a standard numerical simulation. Thus, for all practical purposes the system is in a homogeneous glass phase below the "glass transition line" shown in the phase diagram of Fig. 2.

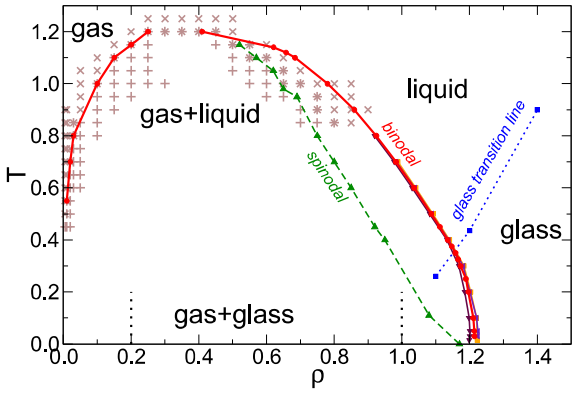

FIG. 2: Temperature-density phase diagram of the binary Lennard-Jones mixture, showing the fluid, liquid and glass homogeneous phases. The "glass transition line" has been obtained from a mode-coupling analysis of the glassy dynamics in the liquid phase [57]. The "binodal" line separates homogeneous from biphasic states. It is obtained by direct inspection of the state points marked by symbols at high temperature, and from the evaluation of the density in the dense phase of biphasic states at low temperature. The "spinodal" line is taken from Ref. [58].

For temperatures below $T_c \approx 1.2$ and low enough densities, $\rho \leq 1.2$, the homogeneous system is unstable and phase coexistence is observed, see Fig. 2. To determine the shown binodal line we have performed quenches to a number of state points (symbols in the figure) and analyze whether the system remains homogeneous at very long times, i.e. we determined whether or not the distribution of coarse-grained density discussed in the previous subsection has only one peak. Very close to the binodal, we payed attention to metastability and hysteretic ef-

fects and performed additional numerical tests to assess the location of the binodal [56]. Unfortunately, this direct method becomes inefficient if temperature becomes small, $T \leq 0.4$, because complete phase separation does not occur in the limited time window of our simulations, and hysteresis effects become more pronounced at lower temperatures. In this region, therefore, the coexistence line has been determined by performing quenches well within the coexistence region, and by measuring the average density of the dense phase of the biphasic configurations, using the method described above in Sec. II B. We have made sure that both methods yield consistent results in the vicinity of $T = 0.4$ where we switch from one approach to the other.

Let us mention here that there exists a controversy in the literature about the nature and the behavior of the coexistence line below its intersection with the bulk glass transition line. While one group claims that the binodal line is little affected by its intersection with the glass transition line [26, 27], another group reports that the density dependence of the binodal evolves non-monotonically with decreasing temperature, and becomes slaved to the glass transition line at low temperatures [28–30]. We shall specifically come back to this point below, and so we describe here only briefly our own findings in Fig. 2, which are somewhat intermediate between the two situations described in the literature. While the binodal line we have determined is not slaved to the glass transition line, its temperature dependence is nevertheless clearly affected by the intersection with this line, so that the measured binodal becomes nearly independent of density at low temperatures, as shown in Fig. 2.

III. QUALITATIVE OVERVIEW OF RESULTS

In this section we present a general overview of the distinct types of morphologies obtained in the course of our numerical studies. We then describe qualitative aspects of the kinetics of the phase separation process at various state points.

A. Biphasic morphologies at long times

We start by discussing the morphologies observed when we quench the system to various state points in the coexistence region of the phase diagram in Fig. 2. Figures 3 and 4 show that for a broad range of densities, $0.2 \leq \rho \leq 1.0$, and for low enough temperatures, $T \leq 0.1$, the morphologies obtained at long times after the quench to the final temperature, $t = 10^4$, are bicontinuous gel-like structures. These particle configurations are strongly reminiscent of the nonequilibrium colloidal gels observed for instance using confocal microscopy [26, 31]. By changing the density and the temperature, the typical length scales characterizing these porous structures change and a central goal of the present paper is to quantify these changes.

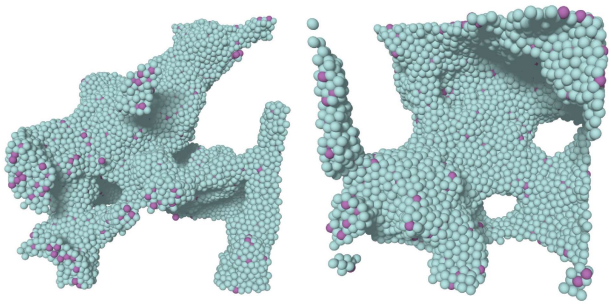

FIG. 3: Snapshots of representative bicontinuous gel-like configurations obtained at long time, $t = 10^4$, for $T = 0.1$ and densities $\rho = 0.2$ (left) and $\rho = 0.6$ (right). For the sake of clarity, these snapshots show only a small fraction (about 16 %) of the total number of particles.

As can be noticed from the snapshots shown in Fig. 3, it is not trivial to visualize the complex morphologies of porous, bicontinuous materials in three dimensions. Therefore, to ease the visualization, we have implemented a numerical method to localize the two phases, and notably the interfaces between them. The procedure relies on the definition of a coarse-grained density field, as explained above in Sec. II B. While we primarily developed this procedure to quantitatively characterize the numerically obtained bicontinuous structures (described below), we find that it is also useful for visualization purposes, as demonstrated in Fig. 4 where now the entire simulation box is shown and the geometries are more easily visualized than by showing particle configurations directly.

In the left column of the figure we show representative configurations obtained at long times for a low temperature, $T = 0.1$ (recall that the critical temperature is $T_c \approx 1.2$) and various densities. For low density, $\rho = 0.15$, one obtains disconnected droplets of dense fluids that slowly coarsen with time. For $\rho \geq 0.2$, a bicontinuous structure is obtained, with a dense phase which occupies an increasing fraction of the total volume as density increases from $\rho = 0.2$, to $\rho = 0.4$ and $\rho = 0.8$. For $\rho \geq 1.0$ (not shown), it is the low-density gas phase which now occupies disconnected bubbles inside the dense phase.

In the right column of Fig. 4 we show the evolution of the final morphology obtained in our simulation for $t = 10^4$ for quenches at fixed intermediate density, $\rho = 0.6$, and different temperatures. While the phase separation proceeds rapidly for shallow quenches, $T \geq 0.5$, it is not complete for a deeper quench at $T = 0.4$, see Fig. 4. (Note that the fact that in this panel the final configuration is not the expected spherical object might also be a finite size effect.) Decreasing further the temperature, $T \leq 0.2$, one observes that even at the end of our simulations an intricate bicontinuous structure remains apparent, indicating that phase separation is far

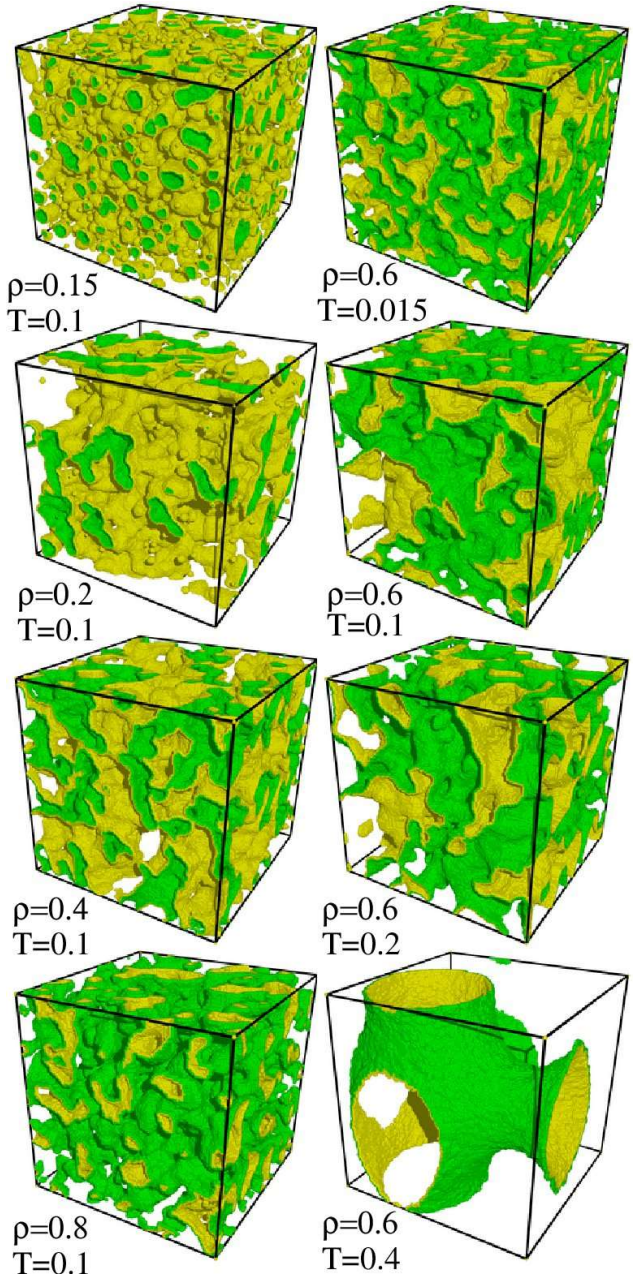

FIG. 4: Representative configurations obtained at long times, $t = 10^4$, and various state points indicated in the figure. Left: constant low temperature, $T = 0.1$, and various densities. Right: constant intermediate density, $\rho = 0.6$, and various temperatures. For all snapshots, periodic boundary conditions are used, as is obvious for instance in the bottom right configuration.

from being reached. Even smaller domains are obtained at large times for very low temperatures, $T = 0.015$. It is therefore clear that at low T the phase separation kinetics is slowed down dramatically and thus the typical domain size remains relatively modest even at very long times. In the subsequent sections of the paper we will characterize these observations in a quantitative manner.

B. Kinetics of phase separation

We now make a qualitative description of the kinetics of the phase separation process at various state points, as illustrated in the time series shown in Fig. 5. Each snapshot in a given row is separated from the previous one by a factor of 10 in time.

The first column in Fig. 5 reproduces the typical time evolution observed in molecular dynamics studies of the liquid-gas spinodal decomposition [6, 10, 48]. For this density, $\rho = 0.4$, the gas and liquid phases occupy similar volumes. The temperature is $T = 0.5$, about half the critical temperature T_c, and thus the quench is not very deep. Using the phase diagram in Fig. 2, we see that the liquid phase is still well above the glass transition line. It thus behaves as a simple liquid, and so the spinodal decomposition takes place with no interference from the physics related to the glass transition. Indeed, one observes that a bicontinuous structure forms over a very short time, $t \approx 10$, and then coarsens slowly with time. For a finite system as the one used in our numerical simulations, the phase separation proceeds until a simple geometry is reached with a flat interface separating the two phases. For an infinite system, of course, spinodal decomposition would proceed indefinitely in a scale-invariant manner [3].

When temperature is decreased to $T = 0.3$ as in the second column in Fig. 5, the initial stages of the phase separation process are little affected and similar bicontinuous structures are formed at early times. This is expected since dynamics at short times mainly results from the well-known spinodal instability [1]: The homogeneous state being fully unstable, a density modulation develops with a dominant wavevector. Therefore, temperature plays little role in this initial process. However, the coarsening dynamics which follows is now clearly affected by the temperature, since the final configuration is no longer a fully demixed system but remains a complex bicontinuous structure. That the coarsening slows down is reasonable since the self-diffusion constant of the dense liquid phase decreases when temperature is lowered, and is expected to be already very small at $T = 0.3$ [52]. On the basis of these snapshots alone, it cannot be decided whether the phase separation kinetics changes nature, or is simply slowed down by a trivial factor in time which could for instance be absorbed in a rescaling t with the diffusion constant. We shall see later that such a simple rescaling is insufficient.

At even lower temperature, $T = 0.1$ (third column in Fig. 5), the situation is much less ambiguous: While the phase separation for early times, $t \leq 10^2$, proceeds as before, the slowing down is now dramatic, as demonstrated by the fact that the two snapshots for $t = 10^3$ and $t = 10^4$ are virtually identical (at least to the eye). This implies that at this temperature phase separation is

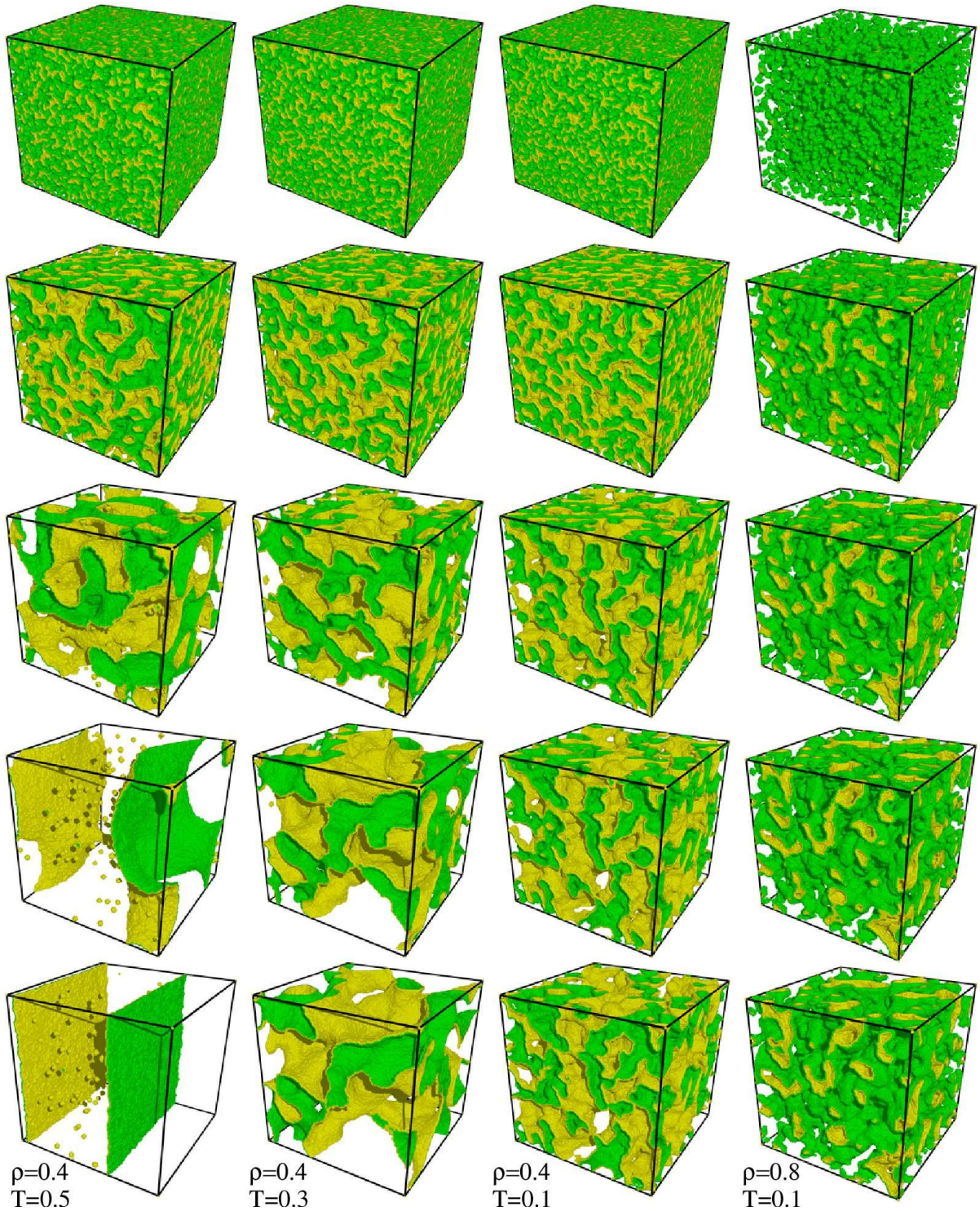

FIG. 5: Time evolution of the phase separating system after a temperature quench at various state points indicated in each column. The selected timescales are identical in the four column. From top to bottom, $t = 1.45$, 13.2, 120, 1096, and 10^4.

nearly arrested at intermediate times, and well before the typical domain size has reached the system size. Finally the fourth column in Fig. 5 illustrates that a similar slowing down of the phase separation is observed for a broad range of densities, the example shown being $\rho = 0.8$ at $T = 0.1$ where again the last two panels look identical but are separated by one order of magnitude in timescales. These observations show that at low temperatures, the domain growth is strongly slowed down, and indicate that the physics of the coarsening process at low temperatures cannot be explained by a simple rescaling of the time scale.

Below, we will establish that the phase separation is in fact not fully arrested at low temperature, but that instead it has changed nature in the sense that the observed growth law depends qualitatively on temperature. Another point that will be carefully considered is whether the near-arrest observed in the low temperature images of Fig. 5 results from a finite size effect, or if it survives in the thermodynamic limit.

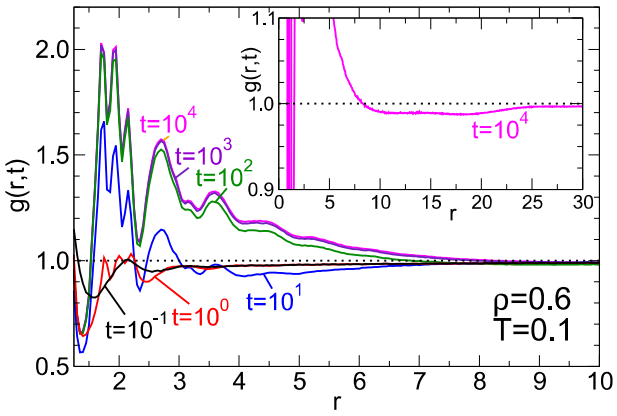

FIG. 6: Time evolution of the pair correlation function $g(r,t)$ for a quench at $\rho = 0.6$ and $T = 0.1$, and various logarithmically separated times. The inset shows a zoom of the small amplitude oscillation around $g(r,t) \approx 1$ which can serve as a measure of the average domain size (see main text for details).

IV. STRUCTURAL ANALYSIS

To quantify the above qualitative observations we must first characterizate the observed bicontinuous structures in terms of quantitative observables and then determine how these depend on time and temperature. In this section we introduce and compare several structural indicators, and show that the so-called "chord length distribution" represents an efficient choice to describe phase separating systems in our particle-based numerical simulations.

A. Pair correlation function

Since we know at each timestep of the simulation the position of all the particles, an obvious choice of a microscopic function to quantity the large scale structures is to record the pair correlation function, defined as [11]

$$g(\mathbf{r},t) = \frac{1}{\rho N} \sum_{j=1}^{N} \sum_{k=1}^{N} \langle \delta(\mathbf{r} - (\mathbf{r}_j(t) - \mathbf{r}_k(t))) \rangle \,, \qquad (4)$$

where the brackets represent an average over independent initial conditions and trajectories, and $\mathbf{r}_j(t)$ is the position of particle j at time t. Since our configurations are isotropic we further perform a spherical average and divide by the phase space factor $4\pi r^2$ to obtain $g(r = |\mathbf{r}|, t)$. We have considered also partial pair correlation functions, specializing the sums in Eq. (4) to either one of the two species of the binary Lennard-Jones mixture. However, since we are interested in the large-scale structure of the configurations, we shall only discuss the total pair correlation described by Eq. (4). Note that the pair correlation function is frequently measured in colloidal experiments using confocal microscopy techniques and hence is a quantity that is experimentally accessible.

In Fig. 6 we show examples of the time evolution of $g(r,t)$ for a quench to $\rho = 0.6$ and $T = 0.1$. By definition, $g(r,t)$ is proportional to the probability to find a particle at distance r from a particle located at the origin. Therefore $g(r,t)$ describes for short distances the local amorphous structure of the dense phase. Accordingly, it shows a pronounced first peak corresponding to interparticle distances (occurring at $r \approx 1.0$ and not shown in the figure), followed by quickly decaying and smooth oscillations representative of an amorphous structure that has no long-range crystalline order.

The difference with a homogeneous liquid appears at larger distances: While in a homogeneous liquid $g(r,t)$ rapidly converges to unity if r increases, for the heterogeneous phase separating systems it shows oscillations around unity even at large distances, as shown in Fig. 6. If t is large, the first oscillation below 1 represents the average distance between a particle taken at random in a dense domain to a neighboring gas region. This physical interpretation suggests that a possible quantitative definition of the average domain size, $L(t)$, can be obtained from $g(L(t),t) = 1$. The data shown in Fig. 6, however, indicate that the oscillations of $g(r,t)$ around unity at large r have a rather small amplitude, in particular if t is large (see Inset in Fig. 6). Our simulations have shown that the above definition is physically sensible, in that it coincides well with the typical domain size seen in the snapshots [56]. However, we also noticed that this measurement is prone to very large statistical fluctuations, since the amplitude of the oscillations in $g(r,t)$ is very small. As a result, the use of this method to follow the

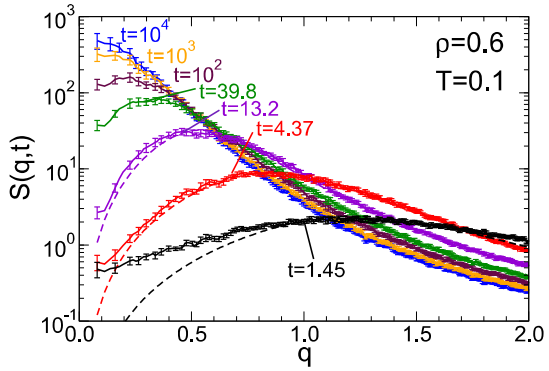

FIG. 7: Time evolution of the static structure factor, Eq. (5), for a quench at $\rho = 0.6$ and $T = 0.1$, and various logarithmically separated times. The lines are fits using Eq. (6).

time evolution of the phase separating systems does require a very large numerical effort since highly accurate pair correlation functions must be measured.

Additional visual inspections indicate that the large distance behavior of $g(r,t)$ is in fact strongly influenced by a small number of very large domains found in the system, whose statistical properties strongly fluctuate from one run to another. Therefore, although this two-point function is a simple structural correlation which corresponds also to the quantity usually analyzed in theoretical calculations, our work suggests that, at least for particle-based numerical simulations, it does not represent the most practical choice to determine the average domain size.

B. Structure factor

Since the static structure factor is the Fourier transform of the pair correlation function [11], it carries *a priori* the same physical content. It is, however, more easily accessible to experiments using for instance light scattering techniques. It is defined as

$$S(\mathbf{q},t) = \frac{1}{N}\sum_{j=1}^{N}\sum_{k=1}^{N}\langle \exp[i\mathbf{q}\cdot(\mathbf{r}_j(t)-\mathbf{r}_k(t))]\rangle\,. \qquad (5)$$

As for the pair correlation function, we perform a spherical average to obtain $S(q,t) = S(|\mathbf{q}|,t)$. In Fig. 7, we show the results for the structure factor for the same set of parameters as for the pair correlation function presented in Fig. 6. An advantage of $S(q,t)$ over the pair correlation function is that the local structure of the dense phase at short-distance and the inhomogeneous bicontinuous structure present at large scales show up in $S(q,t)$ at very different wavevectors and thus can easily be studied independently: While the local structure appears as a sharp peak near $q \approx 2\pi/\sigma \approx 6$, the large domains at larger scale produce a signal at much lower wavevectors, and it is this low-q range which is shown in Fig. 7.

As reported in previous work on spinodal decomposition in fluids [6, 48], the static structure factor develops at low wavevector a peak whose maximum intensity, $S^\star(t)$, grows and whose peak position, $q^\star(t)$, moves to lower q as time increases. The peak position directly reveals the typical domain size in the phase separating system, $L(t) \approx 2\pi/q^\star(t)$, and the q-dependence near the peak can be adjusted using the following empirical formula [59]:

$$S(q,t) = S^\star \frac{3(q/q^\star)^2}{2+(q/q^\star)^6,}, \qquad (6)$$

where the numerical factors are chosen such that $S(q = q^\star,t) = S^\star$. This formula interpolates in a simple manner between the expected quadratic behavior at low q, $S(q \ll q^\star,t) \propto q^2$, and Porod's law describing the structure of the interfaces at larger q, namely $S(q \gg q^\star,t) \propto q^{-4}$, in a three dimensional space. We have used Eq. (6) to fit the data shown in Fig. 7, which gives us direct access to the growing length scale $L(t)$ characterizing the spinodal decomposition.

We have found that this approach is much more reliable to obtain a quantitative estimate of the average domain size than using the function $g(r,t)$, since the large-scale signal is better resolved in Fourier than in real space. Also, we have noticed that fluctuations are less pronounced in $S(q,t)$ than in $g(r,t)$, which implies a reduced numerical effort. The drawback of this simple measurement of the domain size is however readily observed in Fig. 7. Since with increasing time the peak position shifts to lower q, for large t the peak appears at the border of the accessible wavevector range, which is bounded at low q by the system size, i.e. $q \geq \frac{2\pi}{L}$. This is paradoxical at first sight, because the snapshots shown in Fig. 5 seem to indicate that even at large times the average domain size remains quite a bit smaller than the box size.

The reason for this is that the behavior of the structure factor is, just as for the pair correlation function, strongly dominated by the largest domains in the system. Therefore, despite the several advantages mentioned above for the structure factor, it suffers from the practical drawback that accurate measurements of this two-point correlation function require system sizes that are considerably larger than the *typical* domain size. To circumvent this difficulty, we have turned to a slightly more complicated observable, as we now describe.

C. The chord length distribution

The definition of the coarse-grained density field, given by Eq. (3), allows to locate the position of the interfaces separating the two phases in the course of the phase separation process. This information can then be used to

FIG. 8: Chords are defined by the intersection of straight lines with the interfaces in the phase separating system. In this bidimensional example the red segments belong to the dense phase (yellow areas) and their length give the chord length of the dense phase.

measure the distribution of the domain size in the bicontinuous structures.

To this end, we measure the so-called chord length distribution (see Fig. 8) [60, 61]. We define chords by two consecutive intersections of a straight line with the interfaces present in the system. In practice, we measure chords along the three axis of the lattice used to coarse-grain the density, and measure the length ℓ of the segments belonging either to the gas or to the dense phase. For this one has of course to take into account the periodic boundary conditions.

By repeating this measurement over the entire lattice used to determine the coarse-grained density, we obtain the distribution of chord lengths $P(\ell)$, either for chords in the gas phase, or for chords in the dense phase. Representative results for the time evolution of these distributions after a quench to $\rho = 0.6$ and $T = 0.1$ are shown in Fig. 9. These data indicate that, apart the extremely short times when the bicontinuous structure with well-defined interfaces has not yet developed, the two distributions are remarkably similar. They show a maximum, which corresponds to the most probable chord length in each phase, and beyond this length they decay asymptotically with an exponential tail, as observed in many porous media [60, 61]. The sharp peak located near $\ell = L/2$ for the latest time in Fig. 9 is due to finite size effects. Such a clear signature is useful, since it allows to distinguish between measurements that are affected by finite size effects from those which are not.

While either the location of the maximum or the inverse of the slope of the exponential decay can be used as a good quantitative definition of the average domain size, we have decided to gather all the information stemming from the chord length distribution into one single number, and defined the average domain size as the first moment of the distribution:

$$L(t) = \int_0^\infty d\ell \, P(\ell, t)\ell. \qquad (7)$$

In addition, although equivalent at long times, we find that the distribution of chord length in the gas phase yields more accurate results at short times than the one of the dense phase, see Fig. 9. Therefore, in the rest of this paper we shall use Eq. (7) for the chord length distribution in the gas phase as our quantitative determination of the average domain size characterizing our

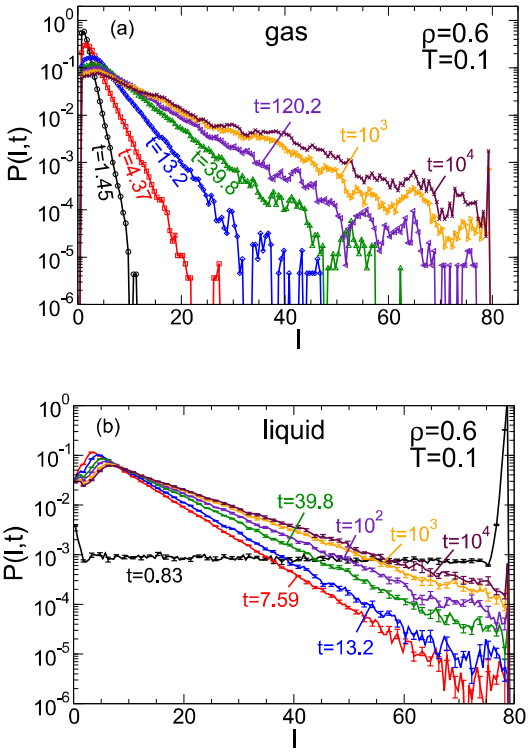

FIG. 9: Time evolution of the chord length distributions measured in the gas phase (a) and in the dense phase (b) after a quench to $\rho = 0.6$ and $T = 0.1$.

phase separating structures.

V. TEMPORAL EVOLUTION

In this subsection, we analyze the temporal evolution of the phase separation process, and study how the kinetics depends on the state point chosen for the quench, focusing in particular on the influence of temperature.

A. Finite size effects

One of the central question we wish to answer is whether or not the phase separation kinetics is arrested at sufficiently low temperatures. In the previous sections we have shown that decreasing T does indeed lead to a strong slowing down of the relaxation dynamics. Before one starts to characterize this slowing down in a more quantitative manner it is, however, important to recall that this relaxation dynamics does depend to some extent on the size of the system and hence one has to check the influence of these finite size effects. In particular, we find that coarsening stops earlier if the systems size is small. The reason for this is that the interfaces are frustrated by the periodic boundary conditions which con-

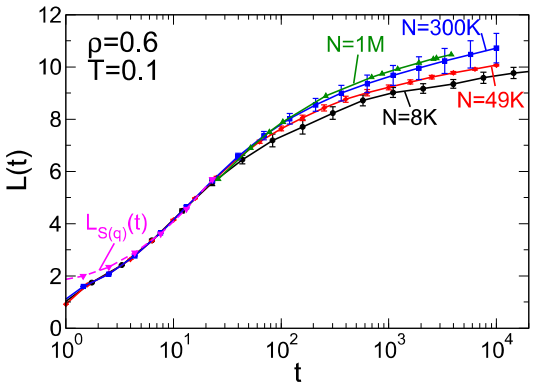

FIG. 10: Influence of system size on the growth of the average domain size for a quench to $\rho = 0.6$ and $T = 0.1$, and system size between $N = 8{\cdot}10^3$ and $N = 10^6$. The data for $L_{S(q)}(t) = 2\pi/q^\star$ are deduced from the analysis of the structure factor shown in Fig. 7. Note that this data has been multiplied by 0.38 in order to match the length scale $L(t)$ at intermediate times.

strain and slow down their motion. This remark is also experimentally relevant for studies of phase separation in confined geometries [62]. Therefore, before concluding on the possibility of kinetically arrested phase separations, it is important to make sure that our results do not depend crucially on the chosen system size.

To this end, we have performed a systematic study of the influence of a finite system size on the growth of the average domain size. Some of these results are presented in Fig. 10 for a quench to $\rho = 0.6$ and $T = 0.1$. These results confirm that the average domain length reached at a given time after the quench increases with increasing the system size. However, we find that this effect does not influence the results in a strong manner. For the particular case shown in Fig. 10, the domain size increases by about 10 % when N increases by more than 2 orders of magnitude. Furthermore we find no N dependence within the error bars for the final sizes shown in Fig. 10. Therefore we have decided to perform most of our studies using $N = 3 \cdot 10^5$, as a compromise between a very large system, and a broad time window in which the dynamics can be probed.

Another finding documented in Fig. 10 is that the growth of the length scale extracted from the chord length distribution, Eq. (7), matches the one obtained from the length scale extracted from the dominant wavevector $q^\star$ in the static structure factor, Eq. (6). In the graph we have multiplied the latter by a constant factor 0.38 and find that at short and intermediate times the two curves do indeed track each other. Thus one can conclude that the chord length distribution represents an efficient and accurate way of extracting the average domain size in phase separating systems.

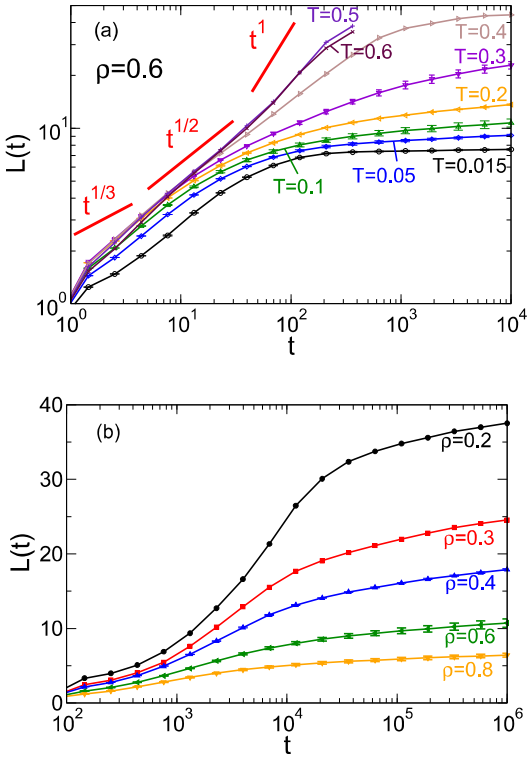

FIG. 11: a) Influence of temperature on the domain growth for $\rho = 0.6$. Various power-laws are included as well. b) Influence of the density on the domain growth for $T = 0.1$.

B. Growth of domain size

We now study how the density and temperature for the quench influence the kinetics of the phase separation process. Our numerical results are summarized in Fig. 11.

We first discuss the influence of temperature for a given density, $\rho = 0.6$, see Fig. 11a. For a relatively shallow quench, $T = 0.5$, the data shows an upward curvature in this double logarithmic representation before it saturates at long times at a system size dependent value, indicating complete phase separation. For relatively early times, the domain growth is approximated well by $L(t) \sim t^{1/2}$, crossing over to a faster growth at larger times before the saturation. Such an apparent square root time dependence has been found in earlier work on the liquid-gas phase separation [6, 48, 49]. Its physical interpretation is that it represents an effective power-law growth [7] interpolating between two regimes, $L(t) \sim t^{1/3}$ at short times followed by $L(t) \sim t$ at longer times, which are theoretically expected power-laws controlling spinodal decomposition at early and late times [5]. These regimes have indeed been separately observed in specifically dedicated simulations [9]. Whereas the first regime corresponds to a surface-tension driven domain growth limited by particle diffusion, the second one is observed when hydrodynam-

ics becomes relevant. We note that our data in Fig. 11 are consistent with this scenario, but do not exhibit convincing power-law regimes over broad and distinct time windows.

The situation for deeper quenches at lower temperature is more unusual. For $T \leq 0.3$ we observe at intermediate times again an algebraic domain growth with an exponent around $1/2$. Since, however, this $t-$dependence crosses over to one that is significantly slower, one cannot argue that the exponent 0.5 is related to a cross-over behavior to the hydrodynamic regime. In fact, due to the very large viscosity of the liquid at low T it must be expected that hydrodynamics ceases to play a role [13]. What is a somewhat surprising is that at long times the growth is even slower than the usual $t^{1/3}$ law. This indicates that at low temperatures surface tension is no longer the main mechanism that drives the coarsening process when the domain size becomes large and that instead a different coarsening regime sets in. This result is in agreement with the snapshots presented in Fig. 3 that show that at low temperatures the interface can be rather rough (see also Fig. 13).

When temperature becomes very small, $T \leq 0.2$, the data in Fig. 11 indicates that the domain growth at long times is not well described by a power-law dependence, as the curves appear to be bent in this log-log representation. This indicates that at these low temperatures the growth is logarithmic, a functional form that is found quite often in glassy systems. For very low temperatures, $T = 0.015$ (which is about 1 % of the critical temperature), the domain size ceases to grow at long times and becomes nearly constant within our statistical accuracy.

The observation of very slow domain growth at low temperature is quite generic, as demonstrated in Fig. 11b, where the density is varied for a constant low temperature $T = 0.1$. The data for $\rho = 0.2$ up to $\rho = 0.8$ basically follow the same time dependence, the rapid initial domain growth becoming logarithmically slow at long times. In contrast to temperature, density has a relatively simple influence on the typical domain size at long times, since to a first approximation denser systems have just smaller domains (see Fig. 5).

The main conclusion of this section is that for deep quenches, i.e. below the glass temperature of the dense phase, the nature of the coarsening process at long times becomes qualitatively different from the standard liquid-gas phase separation. Instead of the usual power-laws we observe a logarithmically slow domain growth, and this domain growth is only fully arrested in the limit of vanishing temperature. This suggests that thermal fluctuations remain relevant and control the slow domain growth during the glass-gas phase separation.

This qualitative change has two important consequences: First, it indicates that the microscopic mechanisms governing the phase separation are different at low temperature from the standard surface tension driven diffusive dynamics observed for shallow quenches. This will be the subject of Sec. VI below. Second, it suggests

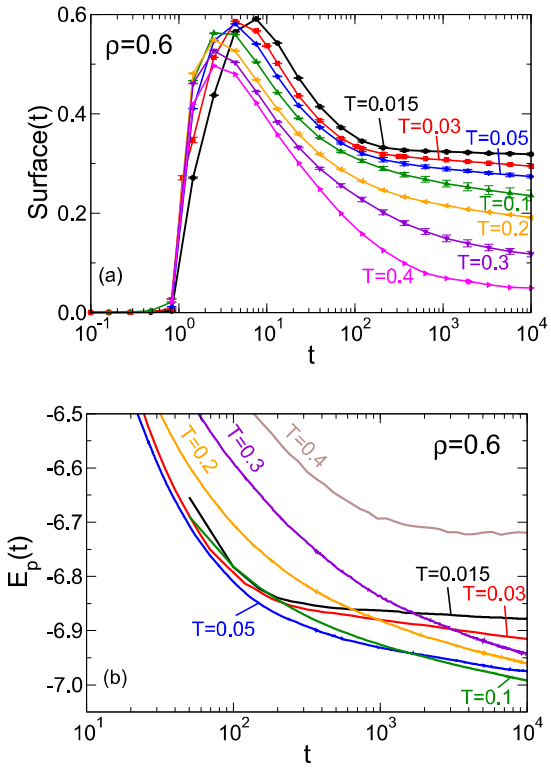

FIG. 12: Time evolution of the surface of the interface (a) and potential energy (b) during the phase separation at $\rho = 0.6$ and various temperatures.

that the reported observation of gels formed by "kinetically arrested" spinodal decomposition in colloidal systems [26, 28] is likely only an approximation (albeit a physically relevant one) resulting from the combination of deep quenches and short observation timescales.

C. Energy density and area of interfaces

Before discussing the details of the microscopic dynamics at low temperature, we present two additional observables that are useful to characterize the dynamics of the system: The energy density and area of interfaces.

The time evolution of these two quantities is shown in Fig. 12 for the density $\rho = 0.6$ and various temperatures. The area of the interface is here expressed as the fraction of the lattice points that are considered as interface, see the coarse-graining procedure described in Sec. II B. Both observables are indicators related to the amount of interfaces in the system, and therefore on how far the phase separation process has advanced. Indeed, the energy density or the amount of topological defects are sometimes used as quantitative indicators of the average domain size during coarsening processes [3].

At short times the $t-$dependence of these two quantities is of course very different: The energy density de-

creases rapidly since it is dominated by the bulk behavior of the fluid which must thermalize at low temperature after the sudden quench from the high temperature. By contrast, because the system must first create a large quantity of interfaces right after the quench from a homogeneous initial state, the amount of interfaces is non-monotonous in that it first increases rapidly at early times, before the coarsening process starts and the surface decreases again, see Fig. 12a.

For times $t > 10$ the evolution of these quantities is more similar, and follows from similar physical considerations. At large times, the area of the interface decreases slowly as a result of the coarsening process which eliminates small domains and generates larger ones. The energy density has a more complicated behavior because it receives contributions from both the energetically costly interfaces as well as from the bulk of the dense domains. Since both contributions decrease slowly with time, the energy density also decreases with increasing t. If one assumes that interfaces dominate the time dependence at long times, then the energy density should display a time dependence that is very similar to the one of the fraction of interfaces, as confirmed by the data in Fig. 12 at high T. However, since we have seen that at low temperatures the size of the domains is not governed by the surface tension (cf. discussion on Fig. 11) one can expect that at low T the time dependence of the energy and of the surface are not the same.

The time dependence of the surface as well as of the energy depends strongly on temperature in that the relaxation becomes slower, in agreement with our findings regarding the size of the domains. Figure 12a shows that the amount of surface at a given (large) time increases monotonically with decreasing temperature, showing that at low T the system has more smaller domains and their surface is rougher. At the lowest temperatures the time dependence of the surface is compatible with a logarithmic decay, in agreement with our results on the growth of the domain sizes.

The increasing fraction of small domains at low temperatures has an implication on the value of the energy at a given (large) time: Since the energy of the dense phase decreases with T, one finds that for intermediate temperatures the energy at large t decreases if T is lowered. However, at even lower T, the system starts to have so many small domains that are rough and that cost energy, that the overall energy starts to increase again, leading to a non-monotonic $T-$dependence of that quantity (see Fig. 12b).

VI. INTERMITTENT DYNAMICS AT LOW TEMPERATURES

In this section we provide evidence that the qualitative change in the growth law at low temperatures is also accompanied by a qualitative evolution of the microscopic mechanisms driving the coarsening dynamics.

A. How domains coarsen

If temperature is not very low, the microscopic dynamics of coarsening is well understood. At early times of the spinodal decomposition, a bicontinuous structure emerges rapidly, which is characterized by a well-defined length scale that reflects the intrinsic instability of the homogeneous system after the quench into the coexistence region. Moreover this bicontinuous structure is characterized by curved interfaces that store a large amount of potential energy. In this case surface tension is the main driving force for the phase separation process that follows the spinodal instability, and domains coarsen in order to reduce the curvature of the interfaces and their total area. At the microscopic scale, this process can proceed because particles can easily move within the dense phase in response to this driving force.

At low temperature, we observe that surface tension becomes unable to advance the coarsening process, because the dense phase is now an (aging) glassy material that has a very high viscosity and is in fact viscoelastic [22, 63]. As a consequence, surface tension is no longer able to relax in a significant manner the curved interfaces formed during the phase separation process.

In a recent experimental work on attractive colloids [33], it has been found that particles located near the interface of the bicontinuous structure have a mobility which is larger than the one of particles in the bulk of the domains. Therefore it has been concluded that surface-enhanced mobility provides an important contribution to the dynamics for deep quenches [33]. We have investigated whether this effect is also relevant for our simulations. First of all we point out that, due to energetic considerations, it is more favorable for the system to put the A particles at the interface (since the A-B interaction is stronger than the A-A interaction). Thus such a micro-segregation would *a priori* give rise to an enhanced mobility of the particles at the interface. However, despite this we have not found that for deep quenches particles at the interfaces are significantly more mobile than the ones inside the dense phase. This result is in fact consistent with earlier studies of the present binary Lennard-Jones in inhomogeneous geometries [64]. While particles near surfaces are in general indeed more mobile than particles in the bulk at equivalent thermodynamic conditions, one should also notice that this dynamical difference is usually only relevant in the narrow range of temperatures which corresponds to the interval between bulk and surface glass temperatures, where bulk diffusion is already arrested while surface diffusion is not. The quench depth should therefore be specifically adjusted to have conditions for which surface-enhanced diffusion is as effective as it seems to be the case in the experiments of Ref. [33].

Although we do find in our low-temperature simulations that slow coarsening persists, this domain growth is driven neither by surface tension nor by interface-enhanced particle diffusion. Instead, the complex bi-

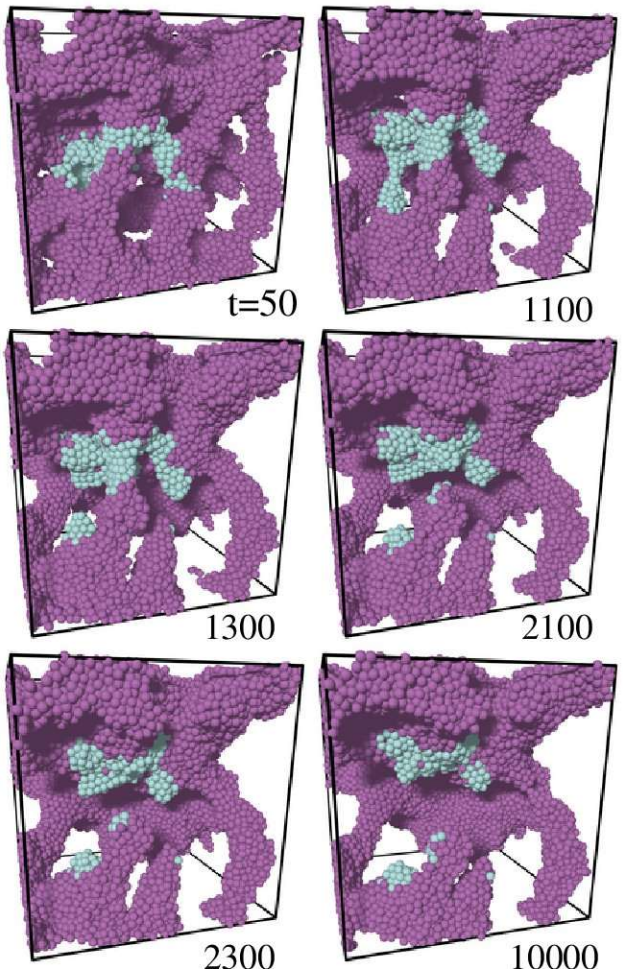

FIG. 13: Time series showing the breaking of two thin domains in a quench at $\rho = 0.4$ $T = 0.1$. Only a small fraction (16 %) of the entire system is shown for clarity, and about 3000 particles with the largest mobility are highlighted, they are located near the breaking points. The first breaking occurs between $t = 50$ and 1100 and the second one between $t = 1300$ and 2100.

continuous structure formed at long times continues to evolve by intermittent breaking of thin necks, which in turn allows the structure to relax further [38, 65]. We illustrate this process in the time series of Fig. 13, where the most mobile particles over the considered time window are highlighted. Visual inspection shows that for this low temperature, $T = 0.1$, particles located at the interface of a dense domain are nearly arrested. A second observation is that the interfaces are relatively rough, which confirms that surface tension is no longer efficient at low temperatures, and that it is unable to relax interfaces that are very curved. A third observation is that the time evolution of the overall structure occurs when thin domains suddenly break, which occurs twice in this specific time series, first near $t \approx 1100$ and then near $t \approx 2100$ in Fig. 13. These sudden events are followed by a slower visco-elastic relaxation of the structure, which eventually gives rise to an increase of the typical domain size.

The reason for this type of relaxation behavior is related to the fact that domains in the bicontinuous structure are under mechanical tension. The stress field present in the glassy structure can be expected to be very inhomogeneous because this is already a characteristic feature in bulk amorphous solids [66] and the presence of a complex geometry will certainly increase this heterogeneity. Due to these stress inhomogeneities and the thermal fluctuations the system will release the stored mechanical stress by breaking domains. These events presumably occur most likely at the weak spots of the structure, i.e. where domains are thin or highly stressed. Once a domain is broken, the system can relax a certain amount of mechanical constraint, and it will reach a new metastable configuration, until another breaking event will occur. This interpretation suggests that it should become more and more difficult to find weak spots to break in the system, or equivalently, that energy barriers that have to be crossed during these events grow with time. This interpretation naturally accounts for a logarithmic growth law for the domain size, as is typically found in many systems with quenched disorder [67].

Interestingly, the qualitative description of the coarsening process occurring in our simulations at low temperatures, which results from the intermittent release of mechanical constraints is reminiscent of the physical scenario put forward by Cipelletti and coworkers to account for the unusual aging dynamics observed via light scattering in a number of soft materials [24, 68, 69]. These researchers put forward the idea that some "internal stress" is stored and intermittently released during the aging process, thus giving rise to the particular relaxation dynamics found in these systems. This analogy suggests that it would be very interesting to study scattering functions for the present system, and compare the results with the behavior reported experimentally using light scattering techniques.

B. Intermittent dynamics in space and time

In this subsection we provide further evidence for a qualitative change in the microscopic dynamics between shallow and deep quenches. In the previous section we have argued that at low T coarsening proceeds by intermittent domain breaking. However, even for shallow quenches domains grow and thin domains can break. The main difference between the two situations is that at low temperatures, mobility is highly localized in space and time, and domain breaking appears very rarely, whereas at high T no such localization is observed.

This difference is illustrated in Figs. 14 and 15, where the 1 % most mobile particles over different time intervals are marked by spheres, and their displacements are represented by a vector. The rest of the particles are

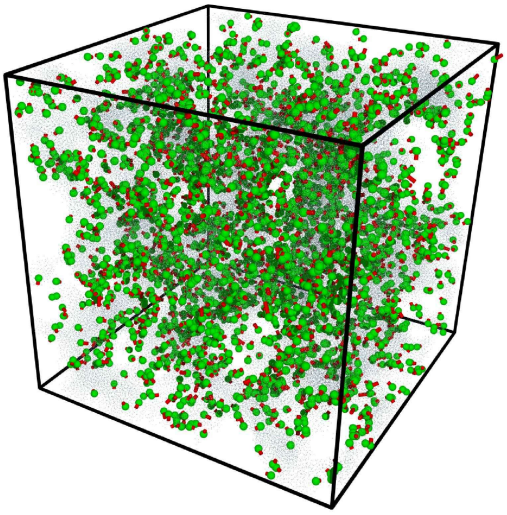

FIG. 14: Most mobile particles (1 % of all particles, shown as spheres) and their displacements (shown as cylinder) for a given time interval, $t \in [38.5, 40.5]$ after a quench to $\rho = 0.4$ and $T = 0.5$.

represented by small dots. The time intervals are chosen so that the images are taken for comparable evolutions of the average domain size. As a consequence, the times are much shorter at the high temperature (Fig. 14) than at the lower one (Fig. 15), and time windows become broader with increasing time in Fig. 15.

At high temperature ($T = 0.5$, Fig. 14) the most mobile particles appear anywhere in the system (both at interfaces and in the bulk domains where mobility is high) and their displacements are essentially uncorrelated. This picture is representative of shallow quenches and indicates that dynamic heterogeneity at the particle scale is not very relevant for ordinary phase separations.

This behavior is in strong contrast with the one found at low temperature, $T = 0.1$ in Fig. 15. In this figure we show mobile particles and their displacements over three different time intervals of the same run, at early, intermediate, and large times. Mobile particles are now clearly clustered, and directly reveal the locations in the system where the geometry of the domains has changed over a given time interval. Furthermore one recognizes that these mobile particles also exhibit highly correlated displacements.

Another remarkable feature is that from one image to the next, clusters of mobile particles appear at different locations, which directly reveals that domain breaking is a spatially and temporally intermittent process. Finally, we notice that mobile particles almost never appear in the interior of the domains, in contrast to the behavior found at high temperatures. Such bulk-like relaxation appears only at very long times, because domain breaking becomes less and less probable as the aging proceeds.

The findings in this subsection suggest that phase separation kinetics for deep quenches is highly intermittent

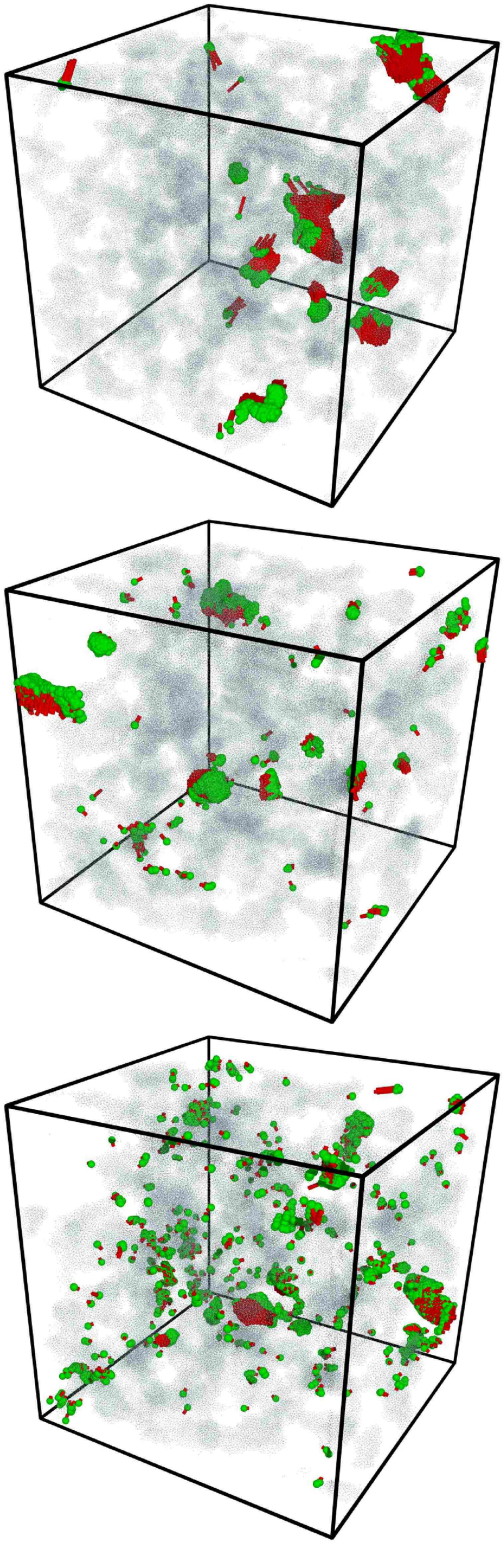

FIG. 15: Most mobile particles (1 % of all particles, shown as spheres) and their displacements (shown as cylinder) for three given time intervals, $t \in [209, 363]$, $t \in [1905, 3311]$, $t \in [5754, 10000]$ (top to bottom), after a quench to $\rho = 0.2$ and $T = 0.1$. The small dots are the remaining 99% of the particles.

in space and time, and should therefore display a high degree of dynamic heterogeneity. It would be interesting to apply the tools developed to study spatially heterogeneous dynamics in glassy materials [70] to quantify further the present observations.

VII. RELATION BETWEEN BINODAL AND GLASS LINES

In this last section, we provide more details and discussion about the determination and behavior of the coexistence line at low temperatures in the phase diagram of Fig. 2.

Why is this an issue? In the phase diagram of Fig. 2, the binodal line crosses the glass transition line near the point $\rho \approx 1.15$ and $T \approx 0.35$. This implies that for temperatures lower than $T = 0.35$, we cannot determine the coexistence line using standard equilibrium simulations, and we have to rely on nonequilibrium protocols to extend the binodal down to $T = 0$. Therefore the low-temperature extension of the coexistence line changes nature at low temperature since it is not uniquely defined anymore but is instead dependent on the protocol.

Because of this difficulty, two experimental groups have investigated this issue in more detail [26, 28]. In both cases the measurements proceed as follows: The system is first quenched into the coexistence region where phase separation takes place, and becomes nearly arrested on experimental timescales. Then the volume occupied by the dense phase is determined experimentally, from which the density is determined. Different methods have been used to measure the evolution of this density as a function of quench depth, and two qualitatively distinct results were found, as mentioned above in Sec. II C.

For the case of our numerical simulations we have followed a similar approach to determine the coexistence line. After quenching the system to a given state point we determined the density of each phase using the coarse-grained density field described in Sec. II B. Following this procedure, we obtained for each configuration both the volume occupied by the dense phase as well as the number of particles it contains, from which the density is easily deduced. Note that for a given temperature, the density of the dense phase will depend in principle on both the time spent since the quench, and on the total density of the system at which the quench has been performed.

In Fig. 16a we demonstrate that after the quench the measured density converges very rapidly to its asymptotic value. This is an important result since it shows that the heterogeneous nature of the configurations does not preclude a quantitative determination of the density of the glass phase. In other words, the time dependence of the glass density is not an issue. Therefore, for a given density, here $\rho = 0.6$, we can vary the quench depth and obtain the temperature evolution of the glass density, which we can include in the $\rho - T$ phase diagram,

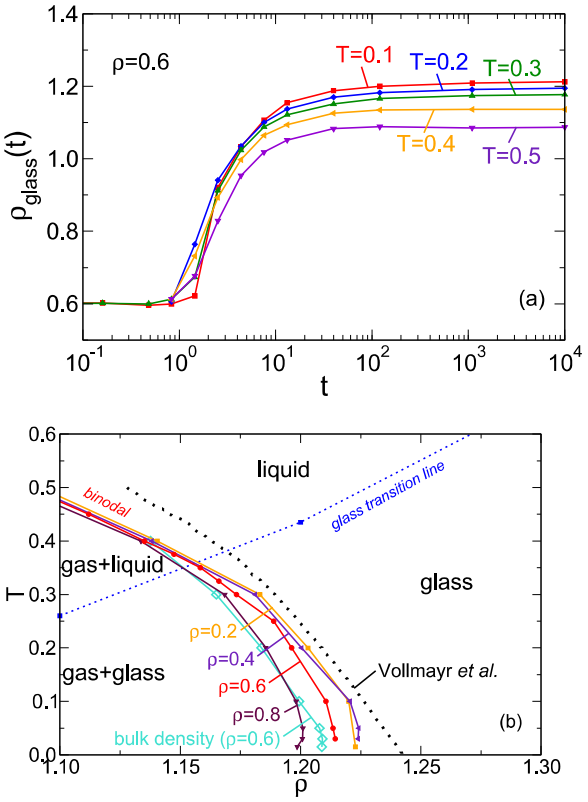

FIG. 16: a) Density of the dense phase during phase separation at $\rho = 0.6$ and various low temperatures. b) Coexistence lines obtained from quenches at various densities are reported in the phase diagram, together with the glass transition line, and the glass density obtained in zero pressure homogeneous glasses in Ref. [71].

see Fig. 16b. In this representation, we focus directly on the relevant temperature region below the intersection with the glass transition line. We observe that the coexistence line determined using quenches at $\rho = 0.6$ changes slightly its curvature at low temperatures, perhaps as a result of crossing the glass transition line, but it is clearly very different from the glass line itself. Therefore our results are closer to the ones of Ref. [26], which determine the density of the glass phase using confocal microscopy and a postprocessing which is not very different from ours. We note that the different results reported in Ref. [28] use a more indirect technique to measure the glass density and the coexistence line.

In Fig. 16b we also document the influence of the quench density on the measured coexistence line, varying the quench density over a broad range between $\rho = 0.2$ and $\rho = 0.8$. We find that all densities produce very similar coexistence lines, with differences in density of about 2 % between the two extremes, the larger quench density producing a smaller glass density.

Finally we compare the results for the coexistence line with a very different numerical approach. In Ref. [71], the

present Lennard-Jones binary mixture was used to study the influence of cooling rates on the structure of the glass. These quenches were done at constant pressure, which was zero. Thus, the produced homogeneous glass configurations were adjusting their densities to maintain a zero pressure, and these densities were recorded numerically. We have included the temperature evolution of these densities in Fig. 16b as well and we see that they compare very well with our determination of the coexistence region. This is expected because the dense phase in our phase separating systems coexists with a gas phase with vanishing pressure. This comparison seems to confirm our finding that the coexistence line does not exhibit a reentrant behavior as a result of the crossing of the glass transition line.

VIII. SUMMARY AND CONCLUSION

We have used large-scale molecular dynamics simulations to study the influence of a temperature quench on the liquid-gas phase separation kinetics in a Lennard-Jones fluid, and therefore the competition between the phase separation kinetics and the glass transition occurring at low temperature in bulk liquids. This represents therefore an example of a viscoelastic phase separation.

Our main finding is the observation that the phase separation kinetics changes qualitatively with decreasing temperature: The microscopic dynamics evolves from a diffusive motion driven by surface tension for shallow quenches, to a qualitatively different coarsening regime in which the dynamics becomes strongly intermittent, spatially heterogeneous and thermally activated at low temperature, leading to logarithmically slow growth of the typical domain size.

The microscopic description of the coarsening process occurring in our simulations at low temperatures, which results from the intermittent release of mechanical constraints, is strongly reminiscent of the physical scenario put forward to explain experimental and simulation results obtained in a broad variety of soft glassy materials for which unusual aging dynamics has been reported [24, 68, 69, 72]. In future work, it would be interesting to compare time correlation functions measured in numerical simulations such as ours to the outcome of light scattering experiments performed in soft glassy materials in their aging regime. Such studies would allow to obtain a better understanding how these soft glass materials are related to the gel-like structures investigated here.

Acknowledgments

We thank D. Reichman for initially stimulating this work, and B. Coasne, T. Gibaud, and P. Royall for useful discussions. The research leading to these results has received funding from the European Research Council under the European Union's Seventh Framework Programme (FP7/2007-2013) / ERC Grant agreement No 306845. W. Kob acknowledges support from the Institut Universitaire de France.

[1] R. C. Desai and R. Kapral, *Dynamics of self-organized and self-assembled structures* (Cambridge University Press, Cambridge, 2009).
[2] M. C. Cross and P. C. Hohenberg, Rev. Mod. Phys. **65**, 851 (1993).
[3] A. J. Bray, Adv. Phys. **43**, 357 (1994).
[4] P. C. Hohenberg and B. I. Halperin, Rev. Mod. Phys **49**, 435 (1977).
[5] H. Furukawa, Adv. Phys. **34**, 703 (1985).
[6] S. W. Koch, R. C. Desai, and F. F. Abraham, Phys. Rev. A **27**, 2152 (1983).
[7] S. Bastea and J. L. Lebowitz, Phys. Rev. Lett. **75**, 3776 (1995).
[8] M. Laradji, S. Toxvaerd, and O. G. Mouritsen, Phys. Rev. Lett. **77**, 2253 (1996).
[9] V. M. Kendon, M. E. Cates, I. Pagonabarraga, J.-C. Desplat, and P. Bladon, J. Fluid Mech. **440**, 147 (2001).
[10] S. Ahmad, S. K. Das and S. Puri, Phys. Rev. E **85**, 031140 (2012).
[11] J. P. Hansen and I. R. McDonald, *Theory of Simple Liquids* (Elsevier, Amsterdam, 1986).
[12] T. A. Witten, *Structured fluids* (Oxford University Press, Oxford, 2004).
[13] H. Tanaka, J. Phys.: Condens. Matter **12**, R207 (2000).
[14] H. Tanaka and Y. Nishikawa, Phys. Rev. Lett. **95**, 078103 (2005).
[15] V. Testard, L. Berthier, and W. Kob, Phys. Rev. Lett. **106**, 125702 (2011).
[16] D. Sappelt and J. Jäckle, Europhys. Lett. **37**, 13 (1997).
[17] S. K. Danchinov, Y. D. Shibanov, and Y. K. Godovsky, Colloid Polym. Sci. **277**, 234 (1999).
[18] F. Varrato, L. Di Michele, M. Belushkin, N. Dorsaz, S. H. Nathan, E. Eiser, and G. Foffi, Proc. Nat. Ac. Science **109**, 19155 (2012).
[19] K. Binder and W. Kob, *Glassy materials and disordered solids* (World Scientific, Singapore, 2011).
[20] L. Berthier and G. Biroli, Rev. Mod. Phys. **83**, 587 (2011).
[21] J.-P. Bouchaud, L.F. Cugliandolo, J. Kurchan, and M. Mézard, Physica A **226**, 243 (1996).
[22] W. Kob and J.-L. Barrat, Phys. Rev. Lett. **78**, 4581 (1997).
[23] L. Buisson, L. Bellon, and S. Ciliberto, J. Phys.: Condens. Mat. **15**, S1163 (2003).
[24] L. Cipelletti and L. Ramos, J. Phys.: Condens. Matter **17**, R253 (2005).
[25] S. Manley, H. M. Wyss, K. Miyazaki, J. C. Conrad, V. Trappe, L. J. Kaufman, D. R. Reichman, and D. A. Weitz, Phys. Rev. Lett. **95**, 238302 (2005).
[26] P. J. Lu, E. Zaccarelli, F. Ciulla, A. B. Schofield, F.

Sciortino, and D. A. Weitz, Nature **453**, 499 (2008).
[27] E. Zaccarelli, P. J. Lu, F. Ciulla, D. A. Weitz, and F. Sciortino, J.Phys.: Condens. Matt. **20**, 494242 (2008).
[28] F. Cardinaux, T. Gibaud, A. Stradner, and P. Schurtenberger, Phys. Rev. Lett. **99**, 118301 (2007).
[29] T. Gibaud and P. Schurtenberger, J. Phys.: Condens. Matt. **21**, 32220 (2009).
[30] T. Gibaud, F. Cardinaux, J. Bergenholtz, A. Stradner, and P. Schurtenberger, Soft Matter **7**, 857 (2011).
[31] A. I. Campbell, V. J. Anderson, J. S. van Duijneveldt, and P. Bartlett, Phys. Rev. Lett. **94**, 208301 (2005).
[32] L. J. Teece, M. A. Faers, and P. Bartlett, Soft Matter **7**, 1341 (2011).
[33] I. Zhang, C. P. Royall, M. A. Faers, and P. Bartlett, Soft matter **9**, 2076 (2013)
[34] G. Foffi, C. de Michele, F. Sciortino, and P. Tartaglia, J. Chem. Phys. **122**, 224903 (2003).
[35] P. Charbonneau and D. Reichman, Phys. Rev. E **75**, 050401(R) (2007).
[36] P. Charbonneau and D. Reichman, Phys. Rev. E **75**, 011507 (2007).
[37] E. Zaccarelli, J. Phys.: Condens. Matter **19**, 323101 (2007).
[38] H. Tanaka and T. Araki, EPL **79**, 58003 (2007).
[39] F. Sciortino and E. Zaccarelli, Curr. Op. Sol. State Mat. Scien. **15**, 246 (2011).
[40] C. P. Royall and S. R. Williams, J. Phys. Chem. B **115**, 7288 (2011).
[41] E. R. Dufresne, H. Noh, V. Saranathan, S. G. J. Mochrie, H. Cao, and R. O. Prum, Soft Matter **5**, 1792 (2009).
[42] J. D. Forster, H. Noh, S. F. Liew, V. Saranathan, C. F. Schreck, L. Yang, J-G Park, R. O. Prum, C. S. O'Hern, S. G. J. Mochrie, H.Cao, and E. R. Dufresne, Adv. Mater. **22**, 2939 (2010).
[43] K. van Gruijthuijsen, V. Herle, R. Tuinier, P. Schurtenberger, and A. Stradner, Soft Matter **8**, 1547 (2012).
[44] W. Ma, C. Yang, X. Gong, K. Lee, and A. J. Heeger, Adv. Funct. Mater. **15**, 1617 (2005).
[45] J. Peet, A. J. Heeger, and G. C. Bazan, Acc. Chem. Res. **42**, 1700 (2009).
[46] J. S. Moon, J. K. Lee, S. Cho, J. Byun, and A. J. Heeger, Nano. Lett. **9**, 230 (2009).
[47] A. Onuki and S. Puri, Phys. Rev. E **59**, 1331 (1999).
[48] R. Yamamoto and K. Nakanishi, Phys. Rev. B **49**, 14958 (1994); Phys. Rev. B **51**, 2715 (1995).
[49] E. Velasco and S. Toxvaerd, Phys. Rev. Lett. **71**, 388 (1993).
[50] B. D. Butler, H. J. M. Hanley, D. Hansen, and D. J. Evans, Phys. Rev. Lett. **74**, 4468 (1995).
[51] J. Sabin, A. E. Bailey, G. Espinosa, and B. J. Frisken, Phys. Rev. Lett. **109**, 195701 (2012).
[52] W. Kob and H. C. Andersen, Phys. Rev. Lett. **73**, 1376 (1994); Phys. Rev. E **51**, 4626 (1995); Phys. Rev. E **52**, 4134 (1995).
[53] S. Plimpton, J. Comp. Phys. **117**, 1 (1995).
[54] S. Majumder and S. K. Das, EPL **95**, 46002 (2011).
[55] S. Ahmad, S. K. Das and S. Puri, Phys. Rev. E **82**, 040107 (2010).
[56] V. Testard, *Etude par simulations numériques de l'influence de la transition vitreuse sur la séparation de phase liquide-gaz*, Thèse de l'Université Montpellier 2 (2011).
[57] L. Berthier and G. Tarjus, Phys. Rev. E **82**, 031502 (2010).
[58] S. Sastry, Phys. Rev. Lett. **85**, 590 (2000).
[59] H. Furukawa, Physica A **123**, 497 (1984).
[60] P. Levitz, Adv. Colloid Interface Sci. **76-77**, 71 (1998).
[61] L. D. Gelb and K. E. Gubbins, Langmuir **14**, 2097 (1998).
[62] P. S. Sarangapani, Y. Yu, J. Zhao, and Y. Zhu, Phys. Rev. E **77**, 061406 (2008).
[63] D. El Masri, L. Berthier, and L. Cipelletti, Phys. Rev. E **82**, 031503 (2010).
[64] R. Malshe, M. D. Ediger, L. Yu, and J. J. de Pablo, J. Chem. Phys. **134**, 194704 (2011).
[65] T. Koyama, T. Araki, and H. Tanaka, Phys. Rev. Lett. **102**, 065701 (2000).
[66] M. Tsamados, A. Tanguy, C. Goldenberg, and J.-L. Barrat, Phys. Rev. E **80**, 026112 (2009).
[67] *Slow Relaxations and Nonequilibrium Dynamics in Condensed Matter*, edited by J.-L. Barrat, J. Dalibard, M. Feigelman, and J. Kurchan (Springer, Berlin, 2003).
[68] L. Cipelletti, S. Manley, R. C. Ball, and D. A. Weitz, Phys. Rev. Lett. **84**, 2675 (2000).
[69] A. Duri, D. A. Sessoms, V. Trappe, and L. Cipelletti, Phys. Rev. Lett. **102**, 085702 (2009).
[70] *Dynamical heterogeneities in glasses, colloids and granular materials*, Eds. L. Berthier, G. Biroli, J.-P. Bouchaud, L. Cipelletti, W. van Saarloos (Oxford University Press, Oxford, 2011).
[71] K. Vollmayr, W. Kob, and K. Binder, J. Chem. Phys. **105**, 4714 (1996).
[72] M.-A. Suarez, N. Kern, E. Pitard, and W. Kob, J. Chem. Phys. **130**, 194904 (2009).